Probing cAMP-Dependent Protein Kinase Holoenzyme Complexes Iα and IIβ by FT-IR and Chemical Protein Footprinting†

Shaoning Yu,‡,§ Fang C. Mei,§,|| J. Ching Lee,‡,§ and Xiaodong Cheng*,§,||

Department of Pharmacology and Toxicology, Department of Human Biological Chemistry and Genetics, and Sealy Center for Structural Biology, School of Medicine, The University of Texas Medical Branch, Galveston, Texas 77555-1031

Received August 12, 2003; Revised Manuscript Received December 4, 2003

ABSTRACT: Although individual structures of cAMP-dependent protein kinase (PKA) catalytic (C) and regulatory (R) subunits have been determined at the atomic level, our understanding of the effects of cAMP activation on protein dynamics and intersubunit communication of PKA holoenzymes is very limited. To delineate the mechanism of PKA activation and structural differences between type I and II PKA holoenzymes, the conformation and structural dynamics of PKA holoenzymes Iα and IIβ were probed by amide hydrogen−deuterium exchange coupled with Fourier transform infrared spectroscopy (FT-IR) and chemical protein footprinting. Binding of cAMP to PKA holoenzymes Iα and IIβ leads to a downshift in the wavenumber for both the α-helix and β-strand bands, suggesting that R and C subunits become overall more dynamic in the holoenzyme complexes. This is consistent with the H−D exchange results showing a small change in the overall rate of exchange in response to the binding of cAMP to both PKA holoenzymes Iα and IIβ. Despite the overall similarity, significant differences in the change of FT-IR spectra in response to the binding of cAMP were observed between PKA holoenzymes Iα and IIβ. Activation of PKA holoenzyme Iα led to more conformational changes in β-strand structures, while cAMP induced more apparent changes in the α-helical structures in PKA holoenzyme IIβ. Chemical protein footprinting experiments revealed an extended docking surface for the R subunits on the C subunit. Although the overall subunit interfaces appeared to be similar for PKA holoenzymes Iα and IIβ, a region around the active site cleft of the C subunit was more protected in PKA holoenzyme Iα than in PKA holoenzyme IIβ. These results suggest that the C subunit assumes a more open conformation in PKA holoenzyme IIβ. In addition, the chemical cleavage patterns around the active site cleft of the C subunit were distinctly different in PKA holoenzymes Iα and IIβ even in the presence of cAMP. These observations provide direct evidence that the R subunits may be partially associated with the C subunit with the pseudosubstrate sequence docked in the active site cleft in the presence of cAMP.

Protein kinases play critical roles in cellular regulation. As a consequence, for proper cell function, protein kinases must be not only specific catalysts but also precisely regulated. They are turned on or off at exact times and locations in response to external signals. cAMP-dependent protein kinase (PKA),[1] the major transducer of the second messenger cAMP in eukaryotic cells, is involved in a myriad of cellular functions, such as metabolism, cell growth, and differentiation. In the absence of the intracellular second messenger cAMP, the catalytic (C) subunit of PKA is sequestered in an inactive state by interacting tightly with the inhibitory regulatory (R) subunit to form a tetrameric holoenzyme (R_2C_2). The binding of cAMP to the R subunit induces a conformational change that leads to dissociation of the holoenzyme into its constituent R and C subunits (*1*, *2*). The free active C subunit can then affect a range of diverse cellular events by phosphorylating target protein substrates that contain the consensus RRX(S/T)Ψ sequences, where X is any amino acid and Ψ is a hydrophobic residue (*3*).

Individual subunit structures of PKA, representing PKA in the active state, have been determined by X-ray crystallography at the atomic level (*4*, *5*). The crystal structure of the C subunit, the first protein kinase structure to be determined, has revealed a common bilobal kinase fold that is shared by all eukaryotic protein kinases. In this structure, the active site lies at the cleft between the two lobes with the adenine ring of ATP deeply buried at the base of the cleft. Most of the invariant residues in the protein kinase core cluster around the active site cleft and contribute to either nucleotide binding or phosphoryl transfer (*4*, *6*). The peptide substrate docks to the surface of the large lobe where the hydroxyl group of the phosphorylation (P) site Ser/Thr is poised for a direct in-line transfer of the γ-phosphate of

† This work was supported by American Cancer Society Research Scholar Grant RSG-01-035-01-TBE, and S.Y. was supported by Robert A. Welch Foundation Grant H-1238.

* To whom correspondence should be addressed. Telephone: (409) 772-9656. Fax: (409) 772-9642. E-mail: xcheng@utmb.edu.

‡ Department of Human Biological Chemistry and Genetics.

§ Sealy Center for Structural Biology.

|| Department of Pharmacology and Toxicology.

[1] Abbreviations: AKAP, A kinase anchoring protein; cAMP, cyclic AMP; PKA, cAMP-dependent protein kinase; C, catalytic subunit of PKA; Caps, 3-(cyclohexylamino)-1-propanesulfonic acid; FT-IR, Fourier transform infrared spectroscopy; Mops, 3-(*N*-morpholino)propanesulfonic acid; PKI, heat stable protein kinase inhibitor; R, regulatory subunit of PKA.

10.1021/bi0354435 CCC: $27.50
Published on Web 01/29/2004

ATP. Crystal structures of the RIα and RII*β* deletion proteins, with the N-terminal dimerization domain removed, have also been determined (*5*, *7*). While these structures reveal the detailed features of each cAMP binding site, little information about how R subunits interact with the C subunit to form the holoenzyme complex has been provided and, consequently, how the binding of cAMP leads to the activation of PKA.

In mammalian cells, there are two isoforms of PKA, designated PKA I and II, due exclusively to differences in the R subunits, RI and RII (*8*). Four different R subunit genes, RIα (*9*), RI*β* (*10*), RIIα (*11*), and RII*β* (*12*), have been identified in humans, while three isoforms of the C subunit (Cα, C*β*, and C*γ*) have been discovered (*13*). Preferential association of any of these C subunits with either RI or RII has not been observed (*14*). Although the ratio of the total R subunits to C subunits in normal tissue has been found to be relatively constant at around 1:1, the relative amount of RI and RII varies and depends highly on physiological conditions and the hormonal status of the tissue (*13*, *15*−*17*). Of the two PKA isoforms, PKA holoenzyme Iα and its regulatory subunit RIα are associated with cell proliferation and neoplastic transformation (*18*, *19*). PKA holoenzyme Iα, required for the G1-to-S transition of the cell cycle, is involved in the epidermal growth factor and transforming growth factor α-mediated mitogenic signaling pathways (*20*−*23*). In hepatoma/fibroblast cell hybrids, RIα, acting as an inhibitor of the expression of several genes related to cell differentiation, has also been identified as the tissue specific extinguisher of differentiation (*24*). These observations correlate very well with the fact that RIα is often overexpressed in human cancer cell lines and in many primary human cancers, such as breast cancer, colon cancer, ovarian cancer, lung cancer, leukemia, and melanoma (*25*−*30*). In contrast, PKA holoenzyme II*β* and its R subunit RII*β* are preferentially expressed in normal tissues, involved in cell growth arrest and differentiation (*25*, *26*, *31*, *32*). Constitutive overexpression of RII*β* induces growth inhibition of human cancer cells and reverts the transformed phenotype of ras-transformed mouse fibroblasts (*33*). Recent studies show that in gene knockout mice lacking the gene encoding RII*β*, the loss of RII*β* in brown fat cells is compensated by an increased level of RIα. The switching of the PKA isoform from $RII\beta_2C_2$ to $RI\alpha_2C_2$ results in an elevated basal level of PKA activity and increasing energy expenditure. The RII*β* knockout mice are leaner and protected against diet-induced obesity (*34*). These results demonstrate clearly that RIα and RII*β*, and therefore their corresponding PKA holoenzymes, are functionally distinct in vivo.

Extensive studies by J. Scott and his colleagues have shown that PKA isoforms are differentially targeted to specific subcellular loci by interacting with a large family of structurally diverse A kinase anchoring proteins, AKAPs (*35*). This isoform specific cellular targeting is likely one of the major factors that are responsible for the isoform specific PKA functions in vivo as AKAPs bring specific PKA isoforms close to a distinct set of substrates at a particular cellular locus. Emerging evidence also suggests that the modes of interaction between the R and C subunits in the type I and II PKA holoenzyme complexes are different (*36*). Such intrinsic structural and/or conformational differences among PKA isoforms not only determine the outcomes of AKAP interactions but also may play a direct role in controlling in vivo PKA functions. Therefore, an understanding of the complex interactions between the R and C subunits in the holoenzyme complexes is essential in further elucidating the function and regulation of PKA. In this study, FT-IR and H−D exchange techniques were applied in examining the structure and dynamics of PKA holoenzyme complexes Iα and II*β*, while chemical protein footprinting was used to probe the interaction between the R and C subunits in the PKA holoenzymes and to identify potential conformational differences between PKA holoenzymes Iα and II*β*.

EXPERIMENTAL PROCEDURES

Materials. The expression vectors used for wild-type murine Cα, bovine RIα, rat RII*β*, and polyhistidine-tagged C were PLWS-3 (*27*), pUC119 (ATCC), pET11c, and pRSET-B (Invitrogen, San Diego, CA), respectively. The following bacterial strains were used for protein expression: *Escherichia coli* BL21-DE3 (C and RII*β*) and *E. coli* E222 (RIα). Horseradish peroxidase-conjugated anti-rabbit IgG (donkey) and an ECL Western blotting detection reagent kit were obtained from Amersham Life Science. All chemicals were reagent-grade.

Protein Purification. The recombinant murine C subunit was isolated from *E. coli* as described previously (*37*). The peak II isozyme was pooled and used for all experiments. Wild-type bovine RIα was purified using DE52 anion exchange chromatography followed by FPLC gel filtration on a Superdex 200 column (Pharmacia), as described previously (*38*). Rat RII*β* was isolated by copurification with H_6-C using a protocol similar to that of Hemmer (*39*). Briefly, equal volumes of *E. coli* cultures that overexpressed RII*β* and H_6-C were mixed and colysed in the presence of 5 mM MgATP. After batch binding of the holoenzyme onto Ni^{2+} resin (Qiagen), the free RII*β* was eluted from the resin with 5 mM cAMP. Pooled fractions from the cAMP elution were precipitated with ammonium sulfate and further purified by FPLC gel filtration on a Superdex 200 column. To obtain cAMP-free R subunits, RIα and RII*β* were dialyzed against 8 M urea to remove cAMP. The chemically denatured R subunit was then refolded back to its folded state by removing urea through dialysis and further purified by passing it through a Superdex 200 gel filtration column (*40*). All proteins were at least 95% pure, as judged by SDS−polyacrylamide gel electrophoresis.

Reconstitution of the PKA Holoenzyme. cAMP-dependent protein kinase holoenzymes were reconstituted from individually purified recombinant C and R subunits. Typically, freshly isolated C and R subunits were mixed in a molar ratio of 1:1.2 and dialyzed against buffer A [10 mM Mops, 50 mM NaCl, and 10 mM $MgCl_2$ (pH 7.2)] extensively at 4 °C to remove cAMP. The dialyzed sample was assayed for PKA activity first in the absence of cAMP and then in the presence of 200 μM cAMP to confirm the formation of the PKA holoenzyme. PKA holoenzyme complexes were further purified using an FPLC Superdex 200 column equilibrated with buffer A. Fractions corresponding to the PKA holoenzyme were collected and concentrated to 8−10 mg/mL using Millipore Ultrafree-4 centrifugal filters. Aliquots of PKA holoenzyme samples in 100 μL fractions were flash-frozen and stored at −80 °C.

FT-IR Spectroscopy. FT-IR spectra were recorded with a Bomem (Quebec, PQ) MB series Fourier transform infrared spectrometer equipped with a dTGS detector and purged constantly with dry air. Protein samples (~10 mg/mL) were warmed to room temperature and loaded in a CaF_2 cell with a 7.5 μm spacer. For each spectrum, a 256-scan interferogram was collected in single-beam mode with a resolution of 4 cm^{-1} at a rate of three scans per second. Reference spectra were recorded under identical conditions with only the corresponding buffer in the cell. Protein spectra were obtained using a previously established protocol (*41*). A straight baseline between 2000 and 1750 cm^{-1} was used as the standard to judge the success of water subtraction. Second-derivative spectra were obtained with a seven-point Savitsky−Golay derivative function, baseline-corrected, and area-normalized as described previously (*41*). The secondary structure content of the PKA holoenzyme was calculated by curve-fitting analysis of the inverted second-derivative spectrum in the amide I band range of 1600−1700 cm^{-1} (*42*). This band is ascribed to the C═O stretching vibration of the peptide bond (*43*). It was assumed that the fraction of residues composing each secondary structure element is proportional to the relative percent area of the associated vibrational band (*44*, *45*).

Measurement of the Level of Hydrogen−Deuterium Exchange. Protein (100 μL) in buffer A was lyophilized for 3 h at room temperature. There was no significant difference in the enzymatic activity and the contents of α-helices and β-sheets between the lyophilized (after rehydration) and unlyophilized proteins measured by the kinetic assay and FT-IR, respectively. Samples for exchange experiments were prepared by dissolving 100 μL of lyophilized PKA holoenzyme or buffer solution with or without 200 μM cAMP in 100 μL of D_2O. The reconstituted sample was injected into a CaF_2 window cell with a path length of 50 μm. One minute after the addition of D_2O, single-beam spectra were recorded using the kinetic scanning mode. FT-IR spectra were recorded at 1, 2, 3, 4, 5, 6, 7, 8, 9, 10, 11, 15, 20, 30, 40, 50, 60, 90, 120, 150, and 180 min. Eight scans were collected for each time interval between 1 and 10 min, while 64 and 128 scans were collected for each time interval between 11 and 90 min and longer, respectively. To compare the FT-IR spectra in H_2O and D_2O, we normalized the amide I band in H_2O to the amide I band in D_2O at 1 min. The spectrum collected after exchange for 24 h was used as the fully deuterated spectrum.

Calculation of the Amide Proton Exchange Rate. We monitored the H−D exchange of PKA holoenzymes by following apparent intensity changes of the amide II band, located around 1548 cm^{-1}, which is attributed to a combination of N−H in-plane bending and C−N stretching vibrations in the peptide bond, because this band does not adversely interfere with absorption bands of H_2O, HOD, or D_2O (*44*). As an N−H bond in protein is changed into an N−D bond in D_2O, the absorption peak of the N−D bending vibration at ~1450 cm^{-1} is strengthened, while the N−H absorption peak decreases. The fraction of unexchanged amide proton, F, was calculated at various time intervals using eq 1

$$F = (A_{II} - A_{II\infty})/A_I\omega \quad (1)$$

where A_I and A_{II} are the absorbance maxima of the amide I and II bands, respectively, $A_{II\infty}$ is the amide II absorbance maximum of fully deuterated PKA, and ω is the ratio of A_{IIo}/A_{Io}, with A_{IIo} and A_{Io} being the absorbance maxima for the amide II and amide I bands of PKA in H_2O, respectively (*46*).

The exchange kinetic parameters were fitted to the equation

$$F = A_1e^{-k_1t} + A_2e^{-k_2t} + C \quad (2)$$

where F is the amide proton fraction at time t, k_1 and k_2 are the intermediate and slow exchange rates, respectively, A_1, A_2, and C are constants, and F_0 is the remaining amide proton fraction at 1 min.

Fe−EDTA Chemical Cleavage Reaction. Chemical cleavage reactions were performed in buffer A at room temperature. A typical reaction mixture (final volume of 50 μL) contained 16 μM purified holoenzyme or C subunit. When present in the reaction mixture, ATP and cAMP were at concentrations of 2 and 1 mM, respectively. The initial reaction mixture (35 μL) was incubated at room temperature for 30 min in a 1.5 mL microcentrifuge tube. The cleavage reaction was started by simultaneously adding 5 μL each of a freshly prepared 1.0 mM 10×$FeSO_4$/2.0 mM EDTA mixture, 20 mM ascorbate (pH adjusted to 7.2), and 1.0 mM H_2O_2 (final concentrations). After the mixture had been incubated for an additional 20 min, the reaction was stopped by adding 17 μL of 4× sample loading buffer [50 mM Tris, 4% SDS, 12% glycerol, 2% β-mercaptoethanol, and 0.01% bromophenol blue (pH 6.8)]. The samples were then applied onto a Tricine-SDS gel for analysis or frozen on a dry ice bath immediately and stored at −80 °C until loading.

Generation of Intrinsic Molecular Markers. Intrinsic molecular markers of the C subunit, generated by partial specific cleavage of the C subunit at Met and Trp residues, were used as molecular standards for calibration of the size of the Fe−EDTA cleavage products. Site specific partial cleavage at methionine residues was achieved by dissolving 100 μg of lyophilized (salt-free) C in 50 μL of 4 mg/mL cyanogen bromide in 70% formic acid. After incubation at room temperature for 30 min, the cleavage reaction was terminated by adding 1 mL of water and was followed by freeze-drying. For site specific partial cleavage at tryptophan residues, 100 μg of C was dissolved in 5.65 μL of 88% formic acid, followed by 40 μL of glacial acetic acid and 4.35 μL of water. The cleavage reaction was initiated by adding 50 μL of 2 mg/mL *N*-chlorosuccinimide in 80% acetic acid. The reaction mixture was incubated at room temperature for 15−60 min, and the reaction was stopped by adding 1 mL of 3 mM methionine and freeze-drying. Dried peptides were dissolved in 50 μL of gel sample buffer right before loading.

Identification and Analysis of Cleavage Products. The cleavage products were analyzed on a 16 cm long, discontinuous Tricine-SDS gel with 16.5% separating, 10% spacing, and 4% stacking gels. The electrophoresis run started at a constant voltage of 30 V, until the protein samples completely entered the gel, and then the voltage was increased to 90−120 V. The run was stopped when the tracking dye reached the bottom of the gel. After electrophoresis, proteins were transblotted onto a PVDF [0.1 μm (Millipore) or 0.2 μm (Bio-Rad)] membrane. Electroblotting was performed in

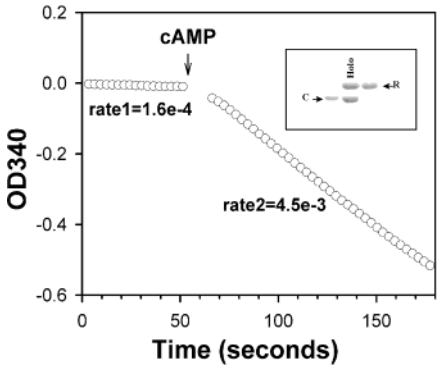

FIGURE 1: Reconstitution of the PKA holoenzyme. The enzymatic activity of PKA holoenzyme Iα reconstituted from purified recombinant R and C subunits was measured spectrophotometrically by a coupled enzyme assay. The reaction rate of 30 nM PKA was determined by following the decrease in absorbance at 340 nm. Approximately 1 min into the reaction, cAMP was added to a final concentration of 200 μM as indicated by the arrow, and the reaction was monitored further for an additional 2 min. The inset shows SDS−PAGE analysis showing a 1:1 ratio of R and C subunits in PKA holoenzyme Iα.

10 mM Caps, 10% methanol (pH 11) buffer at a constant current of 200 mA for 1 h at 4 °C. The membrane was blocked with 5% nonfat milk in TTBS buffer [50 mM Tris, 150 mM NaCl, and 0.1% Tween (pH 7.5)] for 1 h at room temperature or overnight at 4 °C. The membrane was probed with affinity-purified anti-C-terminal C subunit antibodies (*47*) in TTBS buffer containing 5% nonfat milk for 1 h. After three 10 min washes with TTBS buffer, the membrane was further blotted with HRP-conjugated secondary antibody (1:2500) in TTBS buffer containing 5% nonfat milk for 1 h. The membrane was then extensively washed with TTBS buffer (four times for 15 min each) and incubated with ECL reagents for 1−2 min. Protein bands were detected by exposing a sheet of autoradiography film (Hyperfilm-ECL) using the membrane for various times. Once the proper image was obtained, the ECL film was further digitized and analyzed on an Alphaimager 2000 to determine the electrophoretic mobility of the cleavage fragments.

To assign the positions of Fe−EDTA cleavage sites, we ran the Fe−EDTA cleaved sample, along with the partially cleaved peptide fragments (2−5 μL), as molecular weight markers. The measured relative mobilities of these defined C fragments were plotted against their molecular weights. The standard curve was obtained by connecting the neighboring data points on the plot. The molecular weights of the Fe−EDTA cleavage fragments were calculated on the basis of their electrophoretic mobility using the standard curve. The sites of the cleavage were derived using Peptide Tools (Hewlett-Packard) based on their calculated molecular weights.

RESULTS

PKA Holoenzyme Formation. Successful reconstitution of the PKA holoenzyme complex was confirmed by comparing the catalytic activity of the holoenzyme complex in the absence and presence of cAMP. As shown in Figure 1, the catalytic activity of the reconstituted holoenzyme in the absence of cAMP was very low (0.8 s^{-1}) and addition of 200 μM cAMP led to a full activation of the catalytic subunits (24 s^{-1}). This result suggested more than 96% of catalytic subunit is in the form of the holoenzyme when diluted to a final concentration of 30 nM under the assay conditions. Therefore, it is reasonable to conclude that essentially all C subunits are associated with the R subunit in the form of holoenzyme complexes at a much higher concentration (~60 μM) in the reconstituted holoenzyme preparation. Sedimentation velocity analysis of the reconstituted holoenzyme sample showed a single symmetric boundary with an apparent $S_{20,W}$ of 7.0 over an approximately 10-fold range of protein concentrations, while $S_{20,W}$ values of 3.2 and 4.6 were measured for the individual C subunit and R subunit dimer, respectively. In addition, SDS−PAGE showed an approximate 1:1 ratio of R and C subunits in the same holoenzyme preparation (Figure 1, inset). Taken together, these results suggest that the in vitro reconstituted PKA holoenzyme preparations exist in an inactive R_2C_2 tetrameric complex as in cells and can be fully activated by cAMP.

FT-IR Spectra of PKA Iα and IIβ Holoenzyme Complexes in H_2O Solution. The FT-IR absorption spectra of PKA Iα and IIβ holoenzyme complexes in the presence and absence of 200 μM cAMP in buffer A are shown in panels A and B of Figure 2, respectively. The second-derivative amide I spectra of PKA holoenzymes Iα and IIβ (panels C and D of Figure 2, respectively) all exhibited basic band components that can be assigned to secondary structure components. Quantitative analysis of the secondary structure of PKA holoenzyme complexes by curve fitting revealed that PKA holoenzyme Iα contained 35% α-helices, 36% β-strands, 13% β-turns, and 16% 3_{10}-helices while PKA holoenzyme IIβ consisted of 35% α-helices, 37% β-strands, 14% β-turns, and 15% 3_{10}-helices (Figure 3 and Table 1).

Changes in FT-IR Spectra of PKA Iα and IIβ Holoenzyme Complexes Induced by cAMP. Binding of cAMP to PKA holoenzymes Iα and IIβ led to significant changes in FT-IR second-derivative spectra. Both spectra for PKA holoenzymes Iα and IIβ shifted to lower wavenumbers in the presence of cAMP (Figure 2C,D). Interestingly, the secondary structure components of both PKA holoenzymes Iα and IIβ did not change significantly (Table 1), suggesting these apparent changes in FT-IR spectra mainly originated from changes in overall protein dynamics. Although spectra changes in response to cAMP binding were mostly similar, noticeable differences existed between PKA holoenzymes Iα and IIβ. While binding of cAMP induced a shift to lower wavenumbers in the α-helix and β-strand bands for both PKA holoenzymes Iα and IIβ, the degree of the measured downshifts in α-helix and β-strand bands was different between these two holoenzymes. Binding of cAMP to PKA holoenzyme Iα induced a downshift of the β-strand band (2.5 cm^{-1}, from 1638.7 to 1636.2 cm^{-1}) that was more apparent than that of the α-helix band (1.5 cm^{-1}, from 1654.4 to 1652.9 cm^{-1}). In contrast, cAMP led to a 3.0 cm^{-1} (from 1654.4 to 1651.4 cm^{-1}) downshift of the α-helix band and a 1.5 cm^{-1} downshift (from 1638.7 to 1637.2 cm^{-1}) of the β-strand band in PKA holoenzyme IIβ. This ligand-induced shift in the wavenumber of α-helix and β-strand bands reflects an environmental alternation for α-helix and β-strand structures in response to conformational changes at the quaternary and tertiary levels. A similar cAMP-induced downshift in wavenumber from 1676 to 1673 cm^{-1}, as well as a reduction in the intensity of the β-turn band, was

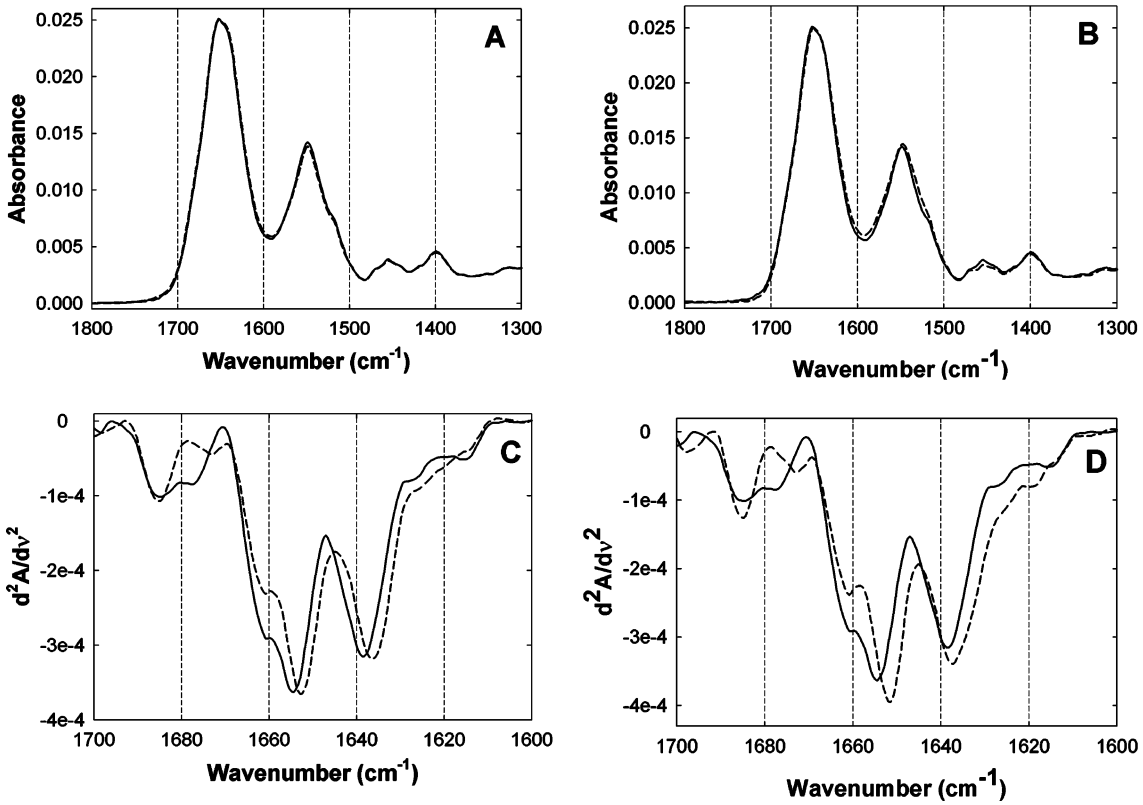

FIGURE 2: FT-IR spectra of PKA holoenzymes in H_2O in the absence and presence of cAMP. Absorption spectra of PKA holoenzymes Iα (A) and IIβ (B). Second-derivative amide I spectra of PKA holoenzymes Iα (C) and IIβ (D). The solid lines depict data for the enzymes without cAMP, and the dashed lines depict data for the enzymes with 200 μM cAMP.

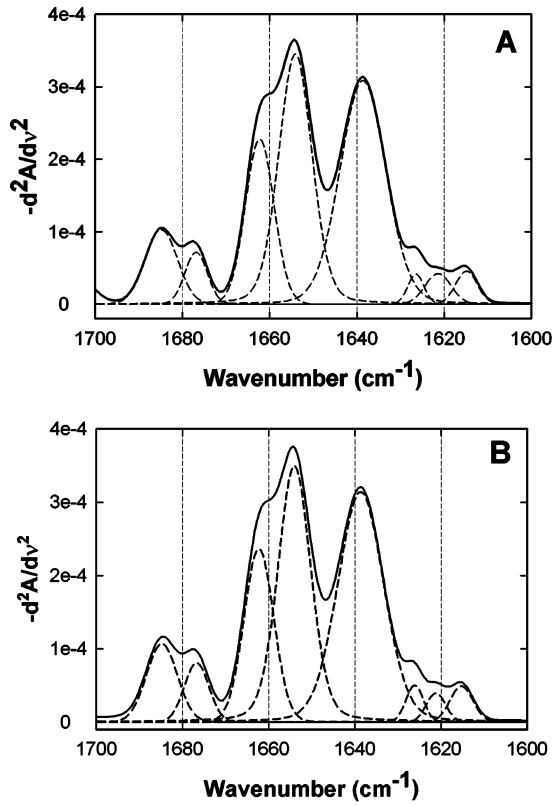

FIGURE 3: Calculation of secondary structure components of PKA holoenzymes. Deconvolution of inverted second-derivative amide I spectra of PKA holoenzymes Iα (A) and IIβ (B).

Table 1: Secondary Structure Contents of PKA Holoenzymes Iα and IIβ Determined by FT-IR[a]

frequency (cm^{-1})	percent	assignment
PKA Holoenzyme Iα without cAMP		
1683.7/1676.1	13.0 ± 0.6	β-turn
1662.3	15.6 ± 1.5	3_{10}-helix
1654.1	35.5 ± 2.4	α-helix
1638.8/1626.8	35.9 ± 1.3	β-strand
PKA Holoenzyme Iα with cAMP		
1684.6/1673.7	10.3 ± 0.7	β-turn
1661.7	14.0 ± 1.2	3_{10}-helix
1652.5	37.6 ± 1.6	α-helix
1636.4/1627.3	38.1 ± 4.1	β-strand
PKA Holoenzyme IIβ Without cAMP		
1685.2/1676.8	13.8 ± 0.9	β-turn
1662.3	14.8 ± 1.2	3_{10}-helix
1654.1	34.7 ± 1.6	α-helix
1638.5/1626.3	36.8 ± 2.2	β-strand
PKA Holoenzyme IIβ with cAMP		
1685.1/1673.4	10.5 ± 0.4	β-turn
1661.5	16.6 ± 1.6	3_{10}-helix
1651.2	33.9 ± 2.1	α-helix
1637.1/1625.1	39.0 ± 2.9	β-strand

[a] Secondary structure contents were obtained from curve fitting of the second-derivative FT-IR spectra using a seven-point Savitsky−Golay derivative function as shown in Figure 3.

observed for both PKA holoenzyme Iα and IIβ complexes. Since the vibrational energy of the amide C═O stretching is inversely related to the strength of hydrogen bonding, the cAMP-induced downshifts in the α-helix, β-strand, and β-turn band wavenumbers imply an overall strengthening in hydrogen bonding within these secondary structure elements when PKA holoenzymes undergo cAMP-induced activation. Moreover, the differential effects of cAMP on α-helix and β-strand bands between PKA holoenzymes Iα and IIβ also suggest that the conformational changes accompanying the

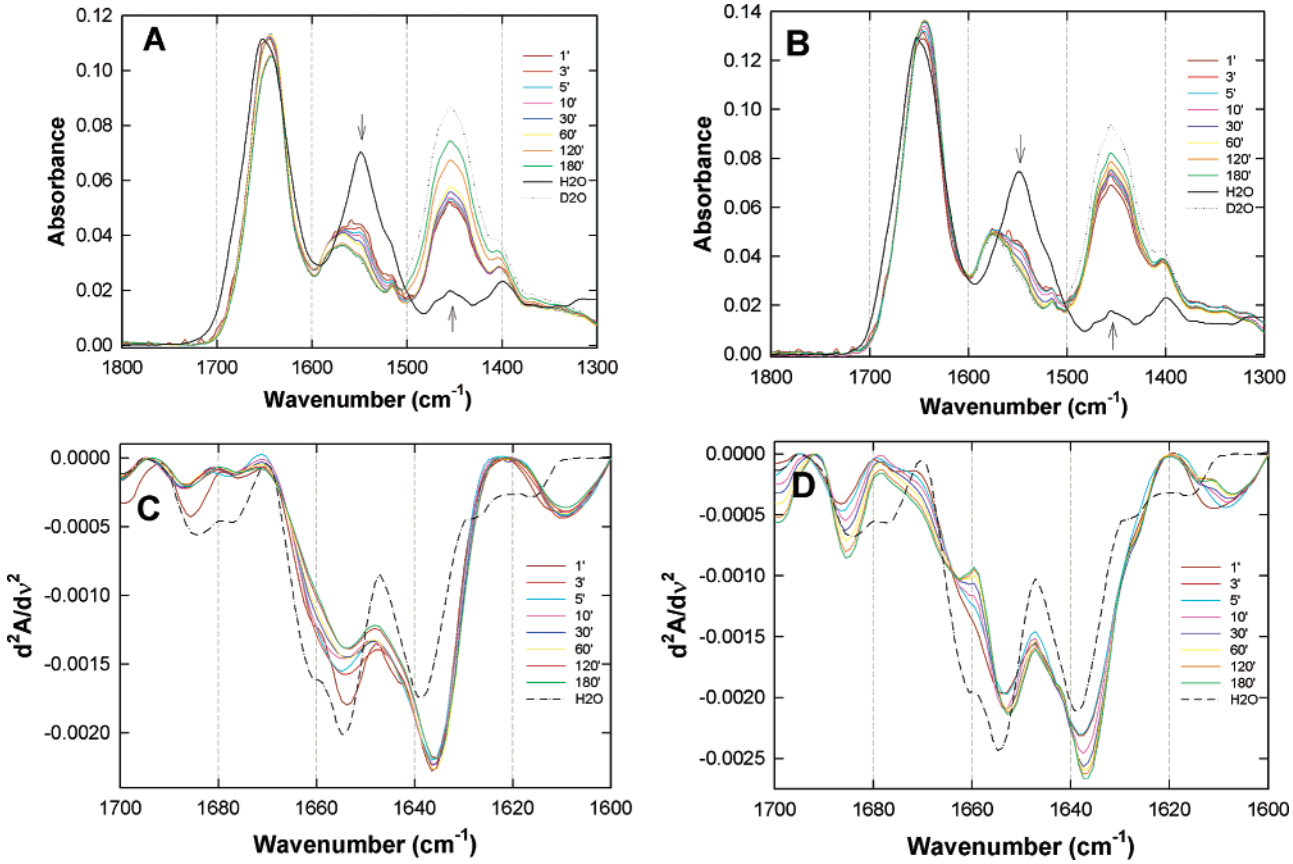

FIGURE 4: H−D exchange in PKA holoenzymes Iα and IIβ as monitored by FT-IR. Infrared spectra of PKA holoenzymes Iα (A) and IIβ (B) at various time intervals after being dissolved in D_2O at room temperature. Second-derivative amide I spectra of PKA holoenzymes Iα (C) and IIβ (D) in D_2O. The spectra of the protein in H_2O and in D_2O after exchange for 24 h depicted with solid and dashed lines, respectively, are included for comparison. Arrows represent the direction of intensity changes.

activation of PKA are distinct between PKA holoenzymes Iα and IIβ.

H−D Exchanges of PKA Iα and IIβ Holoenzyme Complexes Monitored by FT-IR. To explore the intrinsic protein dynamics and general structural features of PKA holoenzyme complexes, H−D exchange of the PKA Iα and IIβ holoenzyme complexes was monitored by FT-IR. Panels A and B of Figure 4 showed an overlay of the representative absorption spectra of PKA holoenzymes Iα and IIβ, respectively, recorded at 1, 3, 5, 10, 15, 30, 60, 120, and 180 min in D_2O with spectra of the proteins in H_2O and fully deuterated in D_2O plotted as references. While the spectra in H_2O exhibited amide I and II band maxima at 1652 and 1548 cm^{-1}, respectively, the spectra of the proteins in D_2O showed a time-dependent isotopic shift of the amide II band from 1548 to 1455 cm^{-1}. This effect is indicative of NH−ND exchange of peptide backbone groups that causes a downshift of approximately 100 cm^{-1} in the vibrational frequency of the amide II band (*48*).

To dissect the overlapping band components of the amide I region, second-derivative analyses were performed. Panels C and D of Figure 4 show an overlay of second-derivative spectra of PKA holoenzymes Iα and IIβ as a function of H−D exchange time, respectively. Almost immediately after the proteins had been dissolved in D_2O, a 2.9 cm^{-1} downshift (from 1638.4 to 1635.5 cm^{-1}) and a concomitant increase in intensity in the major β-sheet band at 1638.4 cm^{-1} were observed for the PKA Iα holoenzyme complex (Figure 4C), whereas the major β-sheet bands of PKA holoenzyme IIβ underwent a gradual increase in intensity and downshift from 1638.4 to 1636.4 cm^{-1} with an increase in exchange time. In addition, the spectral changes of β-sheet bands were more complex for PKA holoenzyme IIβ. There was a noticeable shoulder around 1626 cm^{-1} in D_2O (Figure 4D). The effects of deuterium exchange on the α-helix spectral region were different. The 1655 cm^{-1} band downshifted 1 cm^{-1} to 1654 cm^{-1} and underwent a gradual decrease in intensity with time for the PKA Iα holoenzyme, while the spectral region between 1650 and 1670 cm^{-1} exhibited a complex pattern of change with time for PKA holoenzyme IIβ. An initial large drop in intensity at 1 min of exchange time followed by a gradual relaxation and downshift from 1654.8 to 1652.8 cm^{-1} was observed for the major α-helix band (Figure 4D). The change in intensity for the β-turn region around 1680 cm^{-1} for PKA holoenzyme Iα was immediate. The band intensities at 1684 and 1677 cm^{-1} essentially reached their minima after exchange for 2 min (Figure 4C). The effect of H−D exchange on the β-turn region was significantly different for PKA holoenzyme IIβ compared with the same region in PKA holoenzyme Iα. While there is an immediate decrease in the band intensity of the β-turn region around 1680 cm^{-1}, the 1684 cm^{-1} band intensity of PKA holoenzyme IIβ increased with exchange time after 3 min in D_2O and remained at a level similar to that in H_2O (Figure 4D). In addition to the intensity change, the β-turn band also underwent a gradual upshift in wavenumber from 1683.7 to 1685.7 cm^{-1} (Figure 4C,D). These results suggested while there is a rapid H−D exchange in these β-turns for both PKA

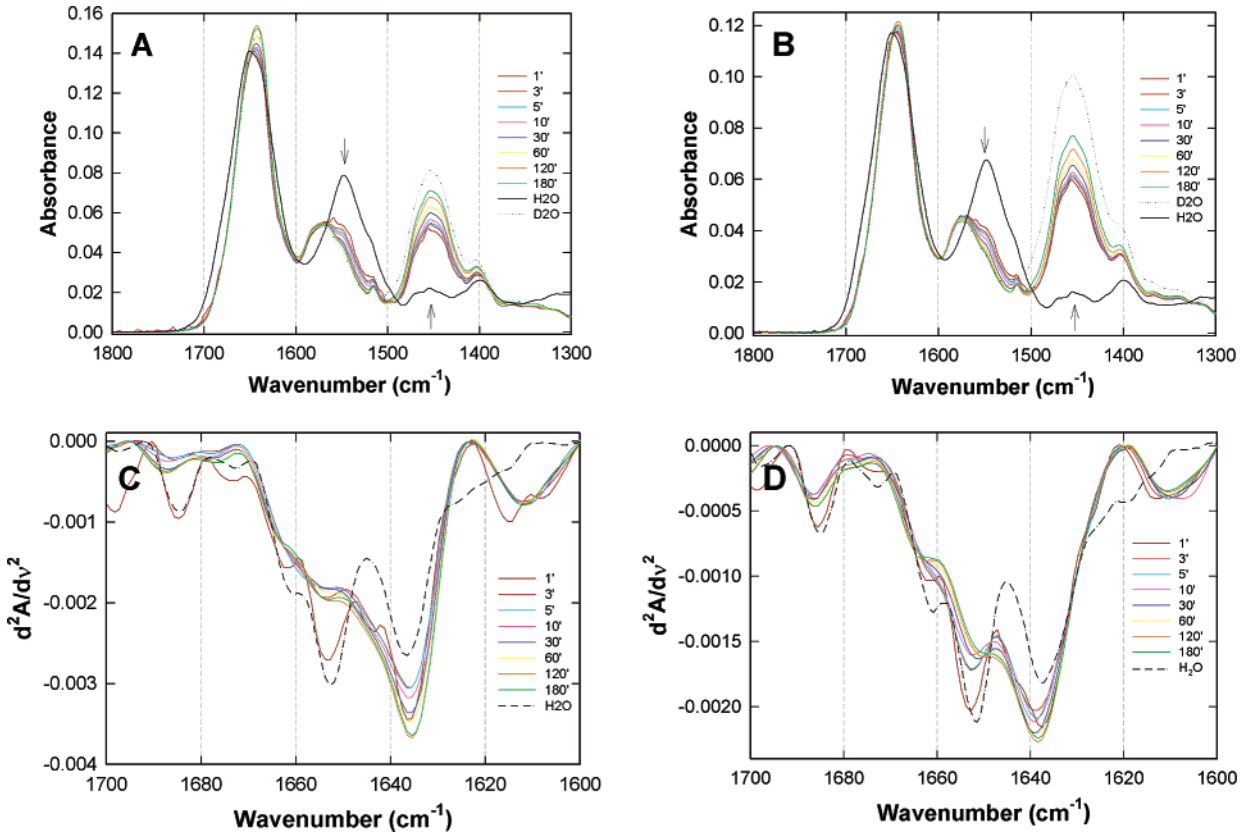

FIGURE 5: H−D exchange in PKA holoenzymes Iα and IIβ in the presence of 200 μM cAMP. Infrared spectra of PKA holoenzymes Iα (A) and IIβ (B) in the presence of 200 μM cAMP at various time intervals after being dissolved in D_2O at room temperature. Second-derivative amide I spectra of PKA holoenzymes Iα (C) and IIβ (D) in the presence of 200 μM cAMP in D_2O. The spectra of the protein in H_2O and D_2O after exchange for 24 h depicted with solid and dashed lines, respectively, are included for comparison. Arrows represent the direction of intensity changes.

holoenzymes Iα and IIβ, the 1685 cm^{-1} β-turn band of PKA holoenzyme IIβ relaxes slowly in D_2O as a function of time.

H−D Exchanges of PKA Iα and IIβ Holoenzyme Complexes in the Presence of cAMP. The overall H−D exchange absorption profiles of PKA holoenzymes Iα and IIβ in the presence of cAMP were very similar to those in the absence of cAMP (Figure 5A,B). However, the second-derivative spectra of H−D exchange in PKA holoenzymes Iα and IIβ in the presence of cAMP were significantly different from those in the absence of the ligand and from each other (Figure 5C,D). Unlike the spectral shifts in the absence of cAMP, a much smaller shift of the major β-sheet component was observed in the presence of cAMP for both PKA holoenzymes Iα and IIβ. In contrast to an immediate 2.9 cm^{-1} downshift (from 1638.4 to 1635.5 cm^{-1}) and increase in intensity in the major β-sheet band in the absence of cAMP, an only 1.0 cm^{-1} shift (from 1636.5 to 1635.5 cm^{-1}) and a gradual increase in intensity of the major β-sheet band were associated with the H−D exchange of the PKA Iα holoenzyme complex in the presence of cAMP (Figure 5C). The position of the major β-sheet band for PKA holoenzyme IIβ in the presence of cAMP remained essentially unchanged as a function of exchange time (Figure 5D). While the major α-helix band of PKA holoenzyme Iα underwent a gradual decrease in intensity and a 1 cm^{-1} downshift in wavenumber, the corresponding band in the presence of cAMP stayed at 1653 cm^{-1} and its intensity fluctuated within a small range after 1 min (Figure 5C). The major α-helix band of PKA holoenzyme IIβ in the presence of cAMP shifted up from 1651.5 to 1652.8 cm^{-1} as compared with a downshift from 1654.8 to 1652.8 cm^{-1} of the same α-helix band in the absence of cAMP (Figure 5D). Finally, the 1685 cm^{-1} β-turn band for both PKA holoenzymes Iα and IIβ decreased in intensity initially after 1 min, reached a minimal value around 5 min, and eventually relaxed gradually as a function of time. The same β-turn band of PKA holoenzyme Iα displayed an upshift in wavenumber (from 1684.7 to 1687.6 cm^{-1}) that was much more apparent than that of PKA holoenzyme IIβ (from 1684.7 to 1685.7 cm^{-1}) (Figure 5C,D).

Differences in Overall H−D Exchange between PKA Holoenzymes Iα and IIβ. The overall H−D exchange rates of PKA holoenzymes Iα and IIβ in the presence and absence of cAMP were estimated by plotting the fraction of unexchanged amide protons, calculated from amide II band data using eq 1, as a function of time. In general, all amide protons in proteins can be divided into three classes (*49*−*51*): (1) fast exchange protons, which are most likely located on the surface of the protein or in regions that are easily accessible to solvent; (2) amide protons with intermediate rates located in flexible buried regions; and (3) the slow exchange fraction located in the core region of the protein. The fractions of unexchanged amide protons at the first exchange time point (1 min) for both PKA holoenzymes Iα and IIβ were around 20% as shown in Figure 6, suggesting that the majority of the amide protons exchanged so rapidly that their exchange was completed within the time interval of the acquisition of the first time point. Therefore, only the intermediate and slow exchange protons can be practically monitored semiquanti-

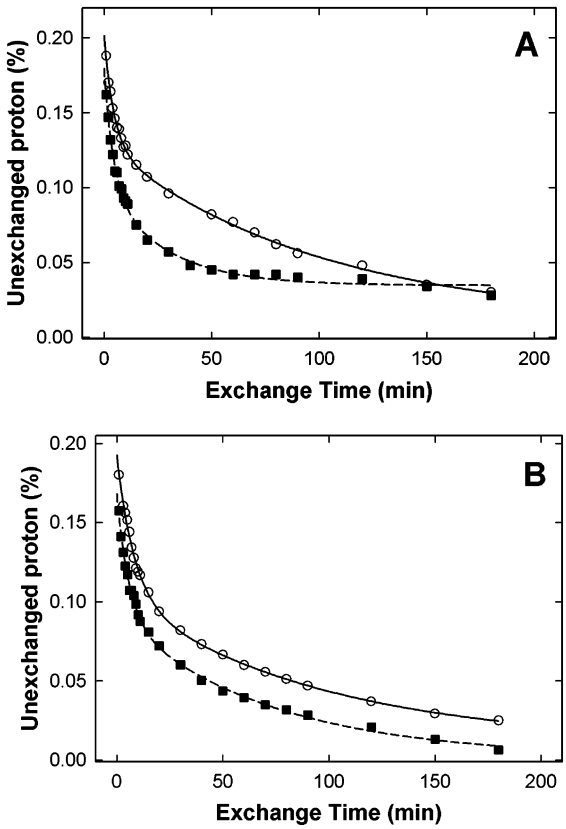

FIGURE 6: Amide proton exchange rates of PKA holoenzymes in the absence (○) and presence (■) of cAMP. Fraction of unexchanged amide protons as a function of exposure time in D_2O for PKA holoenzymes Iα (A) and IIβ (B). The lines represent best fits to the data points using a two-exponential function as described in eq 2.

tatively over the time range employed in this study. A two-exponential decay model (eq 2) was used to describe the exchange reaction of the remaining amide protons within the experimental time frame, and the resolved parameters are summarized in Table 2. Because of the complexity of the overall H−D exchange reaction of the PKA holoenzyme, no attempt was made to quantitatively associate these parameters with any actual physical properties; instead, they were used only qualitatively to assess the overall dynamics of PKA holoenzymes. In the absence of cAMP, the intermediate exchange rate of PKA holoenzyme Iα was ~80% faster than that of PKA holoenzyme IIβ, while the initial percent of unexchanged amide proton (F_0) and the slow exchange rates for PKA holoenzymes Iα and IIβ were similar. These results suggested that the fast exchange rate of PKA holoenzyme IIβ must be faster than that of PKA holoenzyme Iα. In addition, the overall exchange rate in the presence of cAMP was faster than that in the absence of cAMP for both PKA holoenzymes Iα and IIβ. This was reflected from both the amount of remaining unexchanged amide protons (Figure 6) and the estimated exchange rates (Table 2). The most dramatic difference between the inactive and active states was the slow exchange rate of PKA holoenzyme Iα, which in the presence of cAMP was ~3-fold faster than that in the absence of cAMP.

Chemical Protein Footprinting of PKA Holoenzymes. Chemical protein footprinting was used to further probe the intersubunit interaction and structural dynamics of PKA holoenzymes. To monitor the effects of cleavage reagents on the structural and functional integrity of the PKA holoenzyme complex and to ensure that our chemical protein footprinting study of PKA holoenzyme was performed under the optimal "single-cleavage" conditions, we measured the remaining catalytic activity of the PKA holoenzyme in the presence of Fe−EDTA cleavage reagent as a function of time. Incubation of PKA holoenzymes with Fe−EDTA cleavage reagents did not significantly affect the enzymatic activity of the holoenzymes when compared with that of control experiments without cleavage reagents. More than 80 and 95% of the PKA catalytic activity was retained after the enzymes had been treated for 60 and 20 min, respectively. Therefore, for subsequent experiments, we selected a reaction time of 20 min for chemical footprinting of PKA holoenzymes. Under this specific reaction condition, a majority of the PKA holoenzymes remained intact and the likelihood of a single catalytic subunit undergoing more than one hit of cleavage was negligible during the time course of the cleavage reaction (*47*, *52*). Maintaining single-cleavage conditions allows the native conformation of PKA holoenzymes to be probed, rather than the secondary products of a previous cleavage.

The effect of the RIα subunit on chemical cleavage of the C subunit was examined, and the results were compared with those of the free C. Interaction between the R subunit and the C subunit led to a significant change in the cleavage pattern of the C subunit, reflected by significant decreases in susceptibility to Fe−EDTA cleavage in an extensive region of the C subunit (Figure 7A). Furthermore, the apparent protective activities of the C subunit by the R subunit were sensitive to cAMP, and addition of cAMP to the reaction mixture abolished the protecting effect of the R subunit (Figure 7A). These results suggested that interaction between C and RIα subunits in the PKA holoenzyme leads to measurable changes in the solvent accessibility of the C subunit. Furthermore, these changes in cleavage probed by the chemical protein footprinting technique could be modulated by the second messenger, cAMP. Therefore, Fe−EDTA-mediated chemical protein footprinting is a suitable technique for probing structural information of subunit interaction of the PKA holoenzyme complex in a specific and physiologically relevant manner.

Identification of the Subunit Interface between the C and R Subunits. After the single-cleavage footprinting conditions had been established, the interaction between the C and R subunits was monitored by comparing the chemical cleavage patterns of PKA holoenzymes Iα and IIβ in the absence and presence of cAMP. To determine the positions of Fe−EDTA cleavage sites along the primary sequence of the catalytic subunit, we used C subunit peptide fragments partially cleaved at Met and Trp residues as intrinsic molecular standards for calculating the molecular size of the Fe−EDTA cleavage fragments of the C subunit. The locations of the cleavage sites that lead to the formation of these cleavage fragments were then derived from their measured molecular weights. A set of unique cleavage sites was identified in this manner using anti-N- and C-terminal catalytic subunit antibodies in an earlier study (*47*). Binding of the R subunit in the PKA holoenzyme offered significant protection of the C subunit from chemical cleavages at many locations (Figure 7B). Although ECL-based Western blotting is a very sensitive

Table 2: Fitted Exchange Parameters for PKA Holoenzymes Iα & IIβ[a]

	PKA holoenzyme I		PKA holoenzyme II	
parameter[b]	without cAMP	with cAMP	without cAMP	with cAMP
A_1	0.073 ± 0.003	0.079 ± 0.008	0.089 ± 0.005	0.078 ± 0.004
A_2	0.118 ± 0.004	0.062 ± 0.009	0.094 ± 0.004	0.089 ± 0.003
k_1 (min^{-1})	0.219 ± 0.020	0.229 ± 0.043	0.123 ± 0.011	0.174 ± 0.019
k_2 (min^{-1})	0.010 ± 0.001	0.036 ± 0.006	0.010 ± 0.002	0.014 ± 0.002
C	0.010 ± 0.006	0.035 ± 0.002	0.010 ± 0.007	0.002 ± 0.004
F_0	0.201	0.180	0.193	0.168

[a] Parameters were derived from fitting the exchange data in Figure 6 to a two-exponential model as described by eq 2. [b] k_1 and k_2 are the intermediate and slow exchange rates, respectively. A_1, A_2, and C are the constants. F_0 is the remaining amide proton fraction after exposure to D_2O for 1 min.

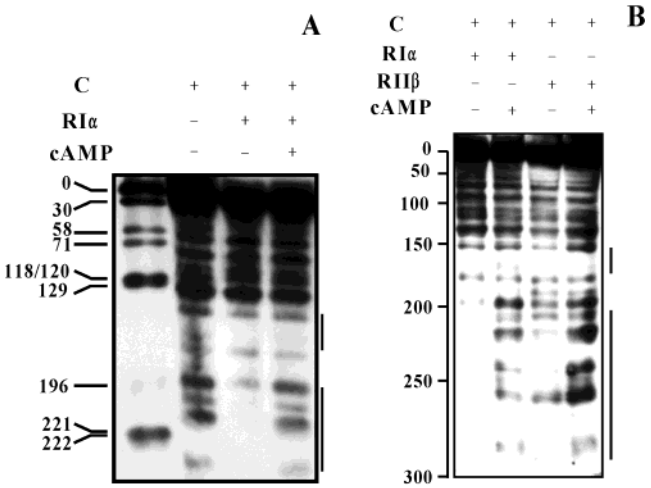

FIGURE 7: Chemical protein footprinting of the PKA holoenzyme. (A) Effect of cAMP on protection of the C Subunit by the RIα subunit: lane 1, partially digested C subunit fragment (visualized with anti-C-terminal C antibodies) generated by Met and Trp specific cleavage at positions 30, 58, 71, 118, 120, 129, 196, and 221/222; lane 2, Fe−EDTA cleavage of the C subunit alone probed by anti-C-terminal antibodies; and lanes 3 and 4, Fe−EDTA cleavage of the PKA holoenzyme Iα complex probed by anti-C-terminal C subunit antibodies in the absence and presence of 1 mM cAMP, respectively. (B) Protein footprinting of PKA holoenzymes Iα and IIβ: lanes 1 and 2, Fe−EDTA cleavage of the C subunit in the PKA Iα holoenzyme complex in the absence and presence of cAMP, respectively; and lanes 3 and 4, Fe−EDTA cleavage of the C subunit in the PKA IIβ holoenzyme complex in the absence and presence of cAMP, respectively. Black bars highlight regions protected by the R subunits in the absence of cAMP.

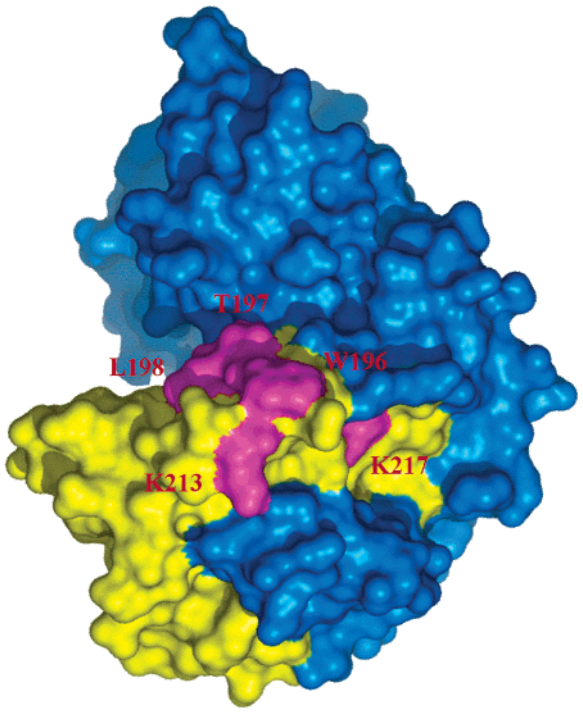

FIGURE 8: Protein surface identified by protein footprinting on the C subunit for docking of the R subunits. Regions of the C subunit (blue) that are protected by the R subunits are highlighted in yellow in the space filling model of the C subunit structure. Residues Trp196, Thr197, Leu198, Lys213, and Lys217 that have been identified previously by genetic screen and biochemical studies as being important for R−C interactions are highlighted in magenta. This figure was drawn with PyMol (DeLano Scientific LLC) using X-ray coordinates for the C subunit (Protein Data Bank entry 1atp).

technique, quantitative interpretation of Western blot data is very difficult. To eliminate potential artifacts due to uneven protein transfer and other limitations intrinsically associated with Western blotting, we performed our chemical footprinting experiments independently seven times. Similar results as shown in Figure 7 with minor variations were obtained. Reliable conclusions can be derived from these multiple footprinting experiments. Differential analysis of the cleavage patterns of PKA footprinting in the presence and absence of cAMP led to the identification of the sites along the C subunit where changes in solvent accessibility occurred upon holoenzyme formation. These protected sites define a large area of the C subunit surface, spanning residues 150−170 and 194−273 (Figure 7B). When these regions were mapped onto the three-dimensional structure of the C subunit, they defined a continuous surface on the C subunit onto which the R subunits could potentially dock (Figure 8). Several residues of the C subunit were identified previously by genetic screens and biochemical studies as being important for R−C interaction: His87, Thr197, Trp196, Leu198, Lys213, and Lys217 (*53*−*56*). All of these residues, except His87 that is located just outside the edge, fall within the region that is defined by protein footprinting in this study (Figure 8).

Although general protection around similar regions of the C subunit was observed in both PKA holoenzymes Iα and IIβ, the detailed cleavage patterns of the C subunit in PKA holoenzymes Iα and IIβ were significantly different, especially in the region around the active site cleft. Overall, the RIα subunit offers much more protection around the active site cleft of the C subunit than does the RIIβ subunit (Figure 7B, lanes 1 and 3). This observation suggests that although RIα and RIIβ most likely recognize the common docking site on the C subunit as defined in Figure 8, the conformation of the C subunit around the active site cleft is different in PKA holoenzymes Iα and IIβ (Figure 7B, lanes 2 and 4). It

was also interesting to note that even in the presence of cAMP the cleavage patterns of the catalytic subunit around the active site cleft were different in PKA holoenzymes Iα and II*β*. This observation suggests that under the experimental conditions, the R subunits may be partially associated with the catalytic subunit with the pseudosubstrate sequences docked in the active site cleft in the presence of cAMP.

DISCUSSION

The cAMP-dependent protein kinase functions as a three-component system consisting of a C subunit, an R subunit, and an activating ligand, cAMP. The inhibitory R subunit interacts with the C subunit with an apparent dissociation constant of <0.2 nM to form the PKA holoenzyme complex (*57*). Such a high-affinity interaction ensures that PKA is kept inactive in the absence of stimuli. The second messenger, cAMP, acts as a signal switch to induce conformational changes in the R subunit and subsequently the destabilization and activation of the holoenzyme complex in response to external cues. To understand the molecular mechanism of PKA activation and isoform specific PKA functions, it is essential to analyze the structure and dynamics of the PKA system in both the active and inactive states, to identify the subunit interface of the PKA holoenzyme, and to compare the conformation similarity and differences between type I and II holoenzyme complexes.

Conformation and Structural Dynamics of PKA Holoenzyme Complexes and Their Modulation by cAMP. Biological functions and their regulation are often associated with changes in protein conformation and dynamics. Amide H−D exchange has been used extensively to analyze structural dynamics and conformational changes in proteins as the rate at which an amide proton exchanges with the solvent is largely determined by the flexibility and motion around the exchanging proton. For both PKA holoenzymes Iα and II*β*, the overall amide protein exchange rates monitored by FT-IR in the absence of cAMP were slightly slower than that in the presence of cAMP (Figure 6). This is not surprising since formation of PKA holoenzyme complexes involves a large intersubunit interface that should render a large number of exchangeable amide protons inaccessible to the solvent. However, the magnitude of the differences in the overall H−D exchange rates of PKA holoenzymes in the presence and absence of cAMP is unexpected. The very small observed differences (<5%) would not be able to fully account for the large extent of the subunit interface of the holoenzyme complex if the overall dynamics of individual subunit in the holoenzyme were kept constant in the presence and absence of cAMP. Therefore, our H−D exchange data suggest that the overall dynamics of the R and C subunits in the PKA holoenzymes complex are greater in magnitude than those of the dissociated R and C subunits in the presence of cAMP. This is further supported by the FT-IR data of PKA holoenzymes in H_2O, in which binding of cAMP to PKA holoenzymes induced a downshift in the wavenumber for both the α-helix and *β*-strand bands (Figure 2). A shift to a lower wavenumber implies a strengthening of the hydrogen bonding network within the α-helix and between the *β*-strands, therefore producing a more tightly packed and less dynamic structure (*58*). In addition, since the C subunit is predominantly α-helical while the R subunit contains mainly *β*-strands, the cAMP-induced wavenumber downshifts in the α-helix and *β*-strand bands further suggest that both R and C subunits become overall more dynamic in the holoenzyme complex.

It is gratifying to note that recent amide H−D exchange mass spectrometry studies of PKA holoenzymes Iα and II*β* suggest that while binding of the C subunit leads to a decrease in the rate of amide hydrogen exchange in the binding interface for both RIα and RII*β* subunits (*59*, *60*), an increase in the rate of amide hydrogen exchange in the other region of the RII*β* subunit is observed (*60*). Specifically, regions adjacent to the pseudosubstrate sites in both RIα and RII*β* and residues 222−244 and 253−268 in cAMP binding domain A of the RIα and RII*β* subunits, respectively, show a decreased solvent accessibility in the holoenzyme complex (*59*, *60*). In contrast, a broad region of cAMP binding domain B along with a small region of cAMP binding domain A (residues 222−232) displays enhanced structural dynamics upon binding the C subunit (*60*). These observations are consistent with our current FT-IR study as the increase in the magnitude of the protein dynamics compensates for the protective effects provided by the formation of the subunit interface and consequently leads to a small difference in the overall hydrogen exchange upon holoenzyme formation.

R−C Subunit Interfaces of PKA Holoenzyme Complexes. The decreased susceptibility of the C subunit to cleavage upon interaction with the R subunit may be due to direct protection of residues that come into physical contact with the R subunit, induced conformational changes associated with R subunit binding, or a combination of both. Although we cannot distinguish between these possibilities by the protein footprint technique, it is reassuring that the majority of amino acid residues identified previously by genetic screens and biochemical studies as being important for PKA holoenzyme formation fall within the surface region that is defined by protein footprinting in this study (Figure 8). Agreement of our chemical footprinting results with those of earlier mutagenesis studies leads us to suggest that the protein surface defined by our protein footprinting study indeed reflects the actual docking surface for the R subunit, which, upon binding to the C subunit, shields the contact surface from cleavage by Fe−EDTA reagents. This docking surface is large and extends to regions on the C subunit that have not been previously implicated in PKA holoenzyme formation. This observation also further confirms that the boundary of R involved in interaction with the C subunit spreads far beyond the consensus inhibitor site, includes the first cAMP binding domain A (*38*), and is consistent with a structural model generated by molecular docking and H−D exchange mass spectrometry (*61*).

The C subunit's docking surface for R subunits revealed by chemical protein footprinting is different from that of the PKI site, as defined in the crystal structure of the C subunit bound to inhibitor peptide PKI(5−24) (*4*, *6*). For PKI, high-affinity binding is achieved by a small, contiguous peptide that includes an amphipathic helix, immediately followed by a pseudosubstrate inhibition segment. This binding surface, termed peripheral recognition site 1 (PRS1), consists of an acidic patch that is important for interaction with the positively charged P-6, P-3, and P-2 Args of PKI and a hydrophobic pocket for docking of the P-11 Phe (*6*). Unlike the interaction between the C subunit and PKI, the R subunit

recognition site on the C subunit is on the opposite side of the active site cleft and involves a much larger surface area (Figure 8). It is clear from the work presented here and earlier studies that the C subunit employs two different surfaces in addition to the common inhibitor recognition site at the active site cleft, to provide high-affinity binding to its two physiological inhibitors, PKI and R subunits. While peripheral recognition site 1 is essential for interaction with PKI, interaction between the R and C subunits involves the docking of the R subunit onto peripheral recognition site 2 (PRS2).

It has been suggested that while activation of the PKA holoenzyme by cAMP weakens the interaction between the R and C subunits, it does not lead to a complete dissociation of the C and R subunits. Part of the R subunit may interact weakly with the C subunit to form a partially associated complex (*62*). Our chemical footprinting results showed that although binding of cAMP reversed a majority of the protections from chemical cleavage on the C subunit provided by the R subunit, the cleavage pattern of the C subunit around the active site was different between PKA holoenzymes Iα and IIβ even in the presence of cAMP. These observations provide direct evidence which suggests that binding of cAMP to the holoenzyme might dissociate the R subunit from the PRS2 site, but not the pseudosubstrate sequence from the active site of the C subunit. Complete dissociation of the R subunit may require the binding of the substrate that replaces the pseudosubstrate sequence of the R subunit from the active site of the C subunit. This conclusion is further supported by analytical ultracentrifugation results that showed more than 80% of the RIIβ (4.6 S) and C subunits (3.2 S) remained in a 7.0 S RIIβ$_2$C$_2$ holoenzyme complex in the presence of cAMP under identical conditions used for our footprinting experiments.

Conformational Differences between Type I and II Holoenzyme Complexes. Although the overall secondary structure contents of PKA holoenzymes Iα and IIβ measured by FT-IR were very similar, changes in FT-IR spectra in response to the binding of cAMP were quite different between PKA holoenzymes Iα and IIβ. Activation of PKA holoenzyme Iα led to more conformational changes in the β-strand structures, while cAMP induced more apparent changes in the α-helical structures in PKA holoenzyme IIβ. This difference in conformational changes associated with PKA activation could arise from the differences in the conformational states between either PKA holoenzymes or individual R subunits. Since RIα and RIIβ share extensive sequence homology and their crystal structures are very similar, it is reasonable to assume that the observed differences in conformational changes upon activation between PKA holoenzymes Iα and IIβ are mainly due to the conformational differences between the PKA holoenzyme Iα and IIβ complexes instead of differences between individual RIα and RIIβ subunits. In addition, the major sequence diversity between RIα and RIIβ is located at the N-terminal dimerization region. Therefore, differential interactions between the N-terminal dimerization domain of RIα and RIIβ and the C subunit are likely the major source of conformational differences in PKA holoenzymes Iα and IIβ. An early site-directed mutagenesis study suggests that the sequence immediately NH_2-terminal to the consensus inhibition site in RIα and RIIβ interacts with different sites at the proximal region of the active site cleft in the C subunit. As a consequence, the N-terminus of RIα is directed to the C-terminal lobe of the C subunit while the N-terminus of RIIβ interacts exclusively with the N-terminal lobe of the C subunit (*36*). Since the small C-terminal lobe of C consists of mostly β-strands while the N-terminal large lobe is exclusively α-helical, it is understandable that the interaction between RIα and C in PKA holoenzyme Iα causes more conformational changes in β-strand structures while interaction between RIIβ and C leads to more structural perturbation in α-helical structures as our FT-IR data suggested.

Consistent with the FT-IR data, our protein footprinting results further extend this mode of differential interaction between RIα and RIIβ and the active site of the C subunit. The active site of the C subunit in PKA holoenzyme Iα is essentially shielded from chemical cleavage, which suggests most likely that the C subunit is in the closed conformation and the pseudosubstrate inhibitor peptide is tightly packed inside the active site cleft. In contrast, the active site of the C subunit in PKA holoenzyme IIβ is much more susceptible to free radical cleavage, which implies that the C subunit in the PKA holoenzyme IIβ complex assumes a more open conformation and the docking of the substrate sequence of RIIβ inside the active site cleft is more loose or dynamic than the pseudosubstrate inhibitor peptide sequence of RIα. An interesting question is whether this difference reflects an intrinsic property of the C subunit in differentiating between peptide substrates and inhibitors. Further study is needed to answer this question. However, a dynamic enzyme−substrate complex is certainly advantageous for efficient enzymatic functions, while maintaining a stable and rigid enzyme−inhibitor complex is important for regulation. Moreover, conformational differences between PKA holoenzymes Iα and IIβ may represent an important mechanism and also provide a structural explanation for isoform specific PKA functions.

REFERENCES

1. Hanks, S. K., Quinn, A. M., and Hunter, T. (1988) The protein kinase family: conserved features and deduced phylogeny of the catalytic domains, *Science 241*, 42−52.
2. Taylor, S. S., Buechler, J. A., and Yonemoto, W. (1990) cAMP-dependent protein kinase: framework for a diverse family of regulatory enzymes, *Annu. Rev. Biochem. 59*, 971−1005.
3. Zetterqvist, Ö. Z., Ragnarsson, U., and Engstrom, L. (1990) in *Peptides and protein phosphorylation* (Kemp, B. E., Ed.) pp 1−41, CRC Press, Boca Raton, FL.
4. Knighton, D. R., Zheng, J. H., Ten Eyck, L. F., Ashford, V. A., Xuong, N. H., Taylor, S. S., and Sowadski, J. M. (1991) Crystal structure of the catalytic subunit of cyclic adenosine monophosphate-dependent protein kinase, *Science 253*, 407−414.
5. Su, Y., Dostmann, W. R., Herberg, F. W., Durick, K., Xuong, N. H., Ten Eyck, L., Taylor, S. S., and Varughese, K. I. (1995) Regulatory subunit of protein kinase A: structure of deletion mutant with cAMP binding domains, *Science 269*, 807−813.
6. Zheng, J., Knighton, D. R., Ten Eyck, L. F., Karlsson, R., Xuong, N., Taylor, S. S., and Sowadski, J. M. (1993) Crystal structure of the catalytic subunit of cAMP-dependent protein kinase complexed with MgATP and peptide inhibitor, *Biochemistry 32*, 2154−2161.
7. Diller, T. C., Madhusudan, Xuong, N. H., and Taylor, S. S. (2001) Molecular basis for regulatory subunit diversity in cAMP-dependent protein kinase: crystal structure of the type II beta regulatory subunit, *Structure 9*, 73−82.
8. Beebe, S. J., and Corbin, J. D. (1986) in *The Enzymes* (Boyer, P. D., and Krebs, E. G., Eds.) pp 43−111, Academic Press, New York.
9. Lee, D. C., Carmichael, D. F., Krebs, E. G., and McKnight, G. S. (1983) Isolation of a cDNA clone for the type I regulatory subunit

of bovine cAMP-dependent protein kinase, *Proc. Natl. Acad. Sci. U.S.A. 80*, 3608−3612.
10. Clegg, C. H., Cadd, G. G., and McKnight, G. S. (1988) Genetic characterization of a brain-specific form of the type I regulatory subunit of cAMP-dependent protein kinase, *Proc. Natl. Acad. Sci. U.S.A. 85*, 3703−3707.
11. Scott, J. D., Glaccum, M. B., Zoller, M. J., Uhler, M. D., Helfman, D. M., McKnight, G. S., and Krebs, E. G. (1987) The molecular cloning of a type II regulatory subunit of the cAMP-dependent protein kinase from rat skeletal muscle and mouse brain, *Proc. Natl. Acad. Sci. U.S.A. 84*, 5192−5196.
12. Jahnsen, T., Hedin, L., Kidd, V. J., Beattie, W. G., Lohmann, S. M., Walter, U., Durica, J., Schulz, T. Z., Schiltz, E., and Browner, M. (1986) Molecular cloning, cDNA structure, and regulation of the regulatory subunit of type II cAMP-dependent protein kinase from rat ovarian granulosa cells, *J. Biol. Chem. 261*, 12352−12361.
13. Doskeland, S. O., Maronde, E., and Gjertsen, B. T. (1993) The genetic subtypes of cAMP-dependent protein kinase: functionally different or redundant? *Biochim. Biophys. Acta 1178*, 249−258.
14. Beebe, S. J., Oyen, O., Sandberg, M., Froysa, A., Hansson, V., and Jahnsen, T. (1990) Molecular cloning of a tissue-specific protein kinase (C gamma) from human testis: representing a third isoform for the catalytic subunit of cAMP-dependent protein kinase, *Mol. Endocrinol. 4*, 465−475.
15. Hofmann, F., Bechtel, P. J., and Krebs, E. G. (1977) Concentrations of cyclic AMP-dependent protein kinase subunits in various tissues, *J. Biol. Chem. 252*, 1441−1447.
16. Sugden, P. H., and Corbin, J. D. (1976) Adenosine 3′:5′-cyclic monophosphate-binding proteins in bovine and rat tissues, *Biochem. J. 159*, 423−427.
17. Lohmann, S. M., and Walter, U. (1984) Regulation of the cellular and subcellular concentrations and distribution of cyclic nucleotide-dependent protein kinases, *Adv. Cyclic Nucleotide Protein Phosphorylation Res. 18*, 63−117.
18. Cho-Chung, Y. S. (1990) Role of cyclic AMP receptor proteins in growth, differentiation, and suppression of malignancy: new approaches to therapy, *Cancer Res. 50*, 7093−7100.
19. Cho-Chung, Y. S., and Clair, T. (1993) The regulatory subunit of cAMP-dependent protein kinase as a target for chemotherapy of cancer and other cellular dysfunctional-related diseases, *Pharmacol. Ther. 60*, 265−288.
20. Tortora, G., Pepe, S., Bianco, C., Baldassarre, G., Budillon, A., Clair, T., Cho-Chung, Y. S., Bianco, A. R., and Ciardiello, F. (1994) The RI alpha subunit of protein kinase A controls serum dependency and entry into cell cycle of human mammary epithelial cells, *Oncogene 9*, 3233−3240.
21. Ciardiello, F., Pepe, S., Bianco, C., Baldassarre, G., Ruggiero, A., Bianco, C., Selvam, M. P., Bianco, A. R., and Tortora, G. (1993) Down-regulation of RI alpha subunit of cAMP-dependent protein kinase induces growth inhibition of human mammary epithelial cells transformed by c-Ha-ras and c-erbB-2 proto-oncogenes, *Int. J. Cancer 53*, 438−443.
22. Ciardiello, F., Tortora, G., Kim, N., Clair, T., Ally, S., Salomon, D. S., and Cho-Chung, Y. S. (1990) 8-Chloro-cAMP inhibits transforming growth factor alpha transformation of mammary epithelial cells by restoration of the normal mRNA patterns for cAMP-dependent protein kinase regulatory subunit isoforms which show disruption upon transformation, *J. Biol. Chem. 265*, 1016−1020.
23. Tortora, G., Damiano, V., Bianco, C., Baldassarre, G., Bianco, A. R., Lanfrancone, L., Pelicci, P. G., and Ciardiello, F. (1997) The RIalpha subunit of protein kinase A (PKA) binds to Grb2 and allows PKA interaction with the activated EGF-receptor, *Oncogene 14*, 923−928.
24. Boshart, M., Weih, F., Nichols, M., and Schutz, G. (1991) The tissue-specific extinguisher locus TSE1 encodes a regulatory subunit of cAMP-dependent protein kinase, *Cell 66*, 849−859.
25. Gordge, P. C., Hulme, M. J., Clegg, R. A., and Miller, W. R. (1996) Elevation of protein kinase A and protein kinase C activities in malignant as compared with normal human breast tissue, *Eur. J. Cancer 32A*, 2120−2126.
26. Bartlett, J. M., Hulme, M. J., and Miller, W. R. (1996) Analysis of cAMP RI alpha mRNA expression in breast cancer: evaluation of quantitative polymerase chain reaction for routine use, *Br. J. Cancer 73*, 1538−1544.
27. Bradbury, A. W., Carter, D. C., Miller, W. R., Cho-Chung, Y. S., and Clair, T. (1994) Protein kinase A (PK-A) regulatory subunit expression in colorectal cancer and related mucosa, *Br. J. Cancer 69*, 738−742.
28. McDaid, H. M., Cairns, M. T., Atkinson, R. J., McAleer, S., Harkin, D. P., Gilmore, P., and Johnston, P. G. (1999) Increased expression of the RIalpha subunit of the cAMP-dependent protein kinase A is associated with advanced stage ovarian cancer, *Br. J. Cancer 79*, 933−939.
29. Beebe, S. J., Salomonsky, P., Holroyd, C., and Becker, D. (1993) Differential expression of cyclic AMP-dependent protein kinase isozymes in normal human melanocytes and malignant melanomas, *Cell Growth Differ. 4*, 1005−1012.
30. Skalhegg, B. S., Johansen, A. K., Levy, F. O., Andersson, K. B., Aandahl, E. M., Blomhoff, H. K., Hansson, V., and Tasken, K. (1998) Isozymes of cyclic AMP-dependent protein kinases (PKA) in human lymphoid cell lines: levels of endogenous cAMP influence levels of PKA subunits and growth in lymphoid cell lines, *J. Cell. Physiol. 177*, 85−93.
31. Tortora, G., Clair, T., and Cho-Chung, Y. S. (1990) An antisense oligodeoxynucleotide targeted against the type II beta regulatory subunit mRNA of protein kinase inhibits cAMP-induced differentiation in HL-60 leukemia cells without affecting phorbol ester effects, *Proc. Natl. Acad. Sci. U.S.A. 87*, 705−708.
32. Rohlff, C., Clair, T., and Cho-Chung, Y. S. (1993) 8-Cl-cAMP induces truncation and down-regulation of the RI alpha subunit and up-regulation of the RII beta subunit of cAMP-dependent protein kinase leading to type II holoenzyme-dependent growth inhibition and differentiation of HL-60 leukemia cells, *J. Biol. Chem. 268*, 5774−5782.
33. Tortora, G., Budillon, A., Yokozaki, H., Clair, T., Pepe, S., Merlo, G., Rohlff, C., and Cho-Chung, Y. S. (1994) Retroviral vector-mediated overexpression of the RII beta subunit of the cAMP-dependent protein kinase induces differentiation in human leukemia cells and reverts the transformed phenotype of mouse fibroblasts, *Cell Growth Differ. 5*, 753−759.
34. Cummings, D. E., Brandon, E. P., Planas, J. V., Motamed, K., Idzerda, R. L., and McKnight, G. S. (1996) Genetically lean mice result from targeted disruption of the RII beta subunit of protein kinase A, *Nature 382*, 622−626.
35. Michel, J. J., and Scott, J. D. (2002) AKAP mediated signal transduction, *Annu. Rev. Pharmacol. Toxicol. 42*, 235−257.
36. Cheng, X., Phelps, C., and Taylor, S. S. (2001) Differential binding of cAMP-dependent protein kinase regulatory subunit isoforms Ialpha and IIbeta to the catalytic subunit, *J. Biol. Chem. 276*, 4102−4108.
37. Herberg, F. W., Bell, S. M., and Taylor, S. S. (1993) Expression of the catalytic subunit of cAMP-dependent protein kinase in *Escherichia coli*: multiple isozymes reflect different phosphorylation states, *Protein Eng. 6*, 771−777.
38. Gibson, R. M., Ji-Buechler, Y., and Taylor, S. S. (1997) Interaction of the regulatory and catalytic subunits of cAMP-dependent protein kinase. Electrostatic sites on the type Ialpha regulatory subunit, *J. Biol. Chem. 272*, 16343−16350.
39. Hemmer, W., McGlone, M., and Taylor, S. S. (1997) Recombinant strategies for rapid purification of catalytic subunits of cAMP-dependent protein kinase, *Anal. Biochem. 245*, 115−122.
40. Buechler, Y. J., Herberg, F. W., and Taylor, S. S. (1993) Regulation-defective mutants of type I cAMP-dependent protein kinase. Consequences of replacing arginine 94 and arginine 95, *J. Biol. Chem. 268*, 16495−16503.
41. Dong, A., and Caughey, W. S. (1994) Infrared methods for study of hemoglobin reactions and structures, *Methods Enzymol. 232*, 139−175.
42. Dong, A., Malecki, J. M., Lee, L., Carpenter, J. F., and Lee, J. C. (2002) Ligand-induced conformational and structural dynamics changes in *Escherichia coli* cyclic AMP receptor protein, *Biochemistry 41*, 6660−6667.
43. Jung, C. (2000) Insight into protein structure and protein−ligand recognition by Fourier transform infrared spectroscopy, *J. Mol. Recognit. 13*, 325−351.
44. Susi, H., and Byler, D. M. (1986) Resolution-enhanced Fourier transform infrared spectroscopy of enzymes, *Methods Enzymol. 130*, 290−311.
45. Dong, A., Huang, P., and Caughey, W. S. (1990) Protein secondary structures in water from second-derivative amide I infrared spectra, *Biochemistry 29*, 3303−3308.
46. Barksdale, A. D., and Rosenberg, A. (1982) Acquisition and interpretation of hydrogen exchange data from peptides, polymers, and proteins, *Methods Biochem. Anal. 28*, 1−113.

47. Cheng, X., Shaltiel, S., and Taylor, S. S. (1998) Mapping substrate-induced conformational changes in cAMP-dependent protein kinase by protein footprinting, *Biochemistry 37*, 14005−14013.
48. Blout, E. R., de Lozé, C., and Asadourian, A. (1961) The Deuterium Exchange of Water-soluble Polypeptides and Proteins as Measured by Infrared Spectroscopy, *J. Am. Chem. Soc. 83*, 1895−1900.
49. Kim, K. S., Fuchs, J. A., and Woodward, C. K. (1993) Hydrogen exchange identifies native-state motional domains important in protein folding, *Biochemistry 32*, 9600−9608.
50. de Jongh, H. H., Goormaghtigh, E., and Ruysschaert, J. M. (1995) Tertiary stability of native and methionine-80 modified cytochrome *c* detected by proton-deuterium exchange using on-line Fourier transform infrared spectroscopy, *Biochemistry 34*, 172−179.
51. Li, J., Cheng, X., and Lee, J. C. (2002) Structure and dynamics of the modular halves of *Escherichia coli* cyclic AMP receptor protein, *Biochemistry 41*, 14771−14778.
52. Brenowitz, M., Senear, D. F., Shea, M. A., and Ackers, G. K. (1986) Quantitative DNase footprint titration: a method for studying protein-DNA interactions, *Methods Enzymol. 130*, 132−181.
53. Levin, L. R., Kuret, J., Johnson, K. E., Powers, S., Cameron, S., Michaeli, T., Wigler, M., and Zoller, M. J. (1988) A mutation in the catalytic subunit of cAMP-dependent protein kinase that disrupts regulation, *Science 240*, 68−70.
54. Levin, L. R., and Zoller, M. J. (1990) Association of catalytic and regulatory subunits of cyclic AMP-dependent protein kinase requires a negatively charged side group at a conserved threonine, *Mol. Cell. Biol. 10*, 1066−1075.
55. Orellana, S. A., and McKnight, G. S. (1992) Mutations in the catalytic subunit of cAMP-dependent protein kinase result in unregulated biological activity, *Proc. Natl. Acad. Sci. U.S.A. 89*, 4726−4730.
56. Orellana, S. A., Amieux, P. S., Zhao, X., and McKnight, G. S. (1993) Mutations in the catalytic subunit of the cAMP-dependent protein kinase interfere with holoenzyme formation without disrupting inhibition by protein kinase inhibitor, *J. Biol. Chem. 268*, 6843−6846.
57. Francis, S. H., and Corbin, J. D. (1994) Structure and function of cyclic nucleotide-dependent protein kinases, *Annu. Rev. Physiol. 56*, 237−272.
58. Krimm, S., and Bandekar, J. (1986) Vibrational spectroscopy and conformation of peptides, polypeptides, and proteins, *Adv. Protein Chem. 38*, 181−364.
59. Anand, G. S., Hughes, C. A., Jones, J. M., Taylor, S. S., and Komives, E. A. (2002) Amide H/^{2}H exchange reveals communication between the cAMP and catalytic subunit-binding sites in the R(I)alpha subunit of protein kinase A, *J. Mol. Biol. 323*, 377−386.
60. Hamuro, Y., Zawadzki, K. M., Kim, J. S., Stranz, D. D., Taylor, S. S., and Woods, V. L., Jr. (2003) Dynamics of cAPK type IIbeta activation revealed by enhanced amide H/2H exchange mass spectrometry (DXMS), *J. Mol. Biol. 327*, 1065−1076.
61. Anand, G. S., Law, D., Mandell, J. G., Snead, A. N., Tsigelny, I., Taylor, S. S., Ten Eyck, L. F., and Komives, E. A. (2003) Identification of the protein kinase A regulatory RIalpha-catalytic subunit interface by amide H/^{2}H exchange and protein docking, *Proc. Natl. Acad. Sci. U.S.A. 100*, 13264−13269.
62. Yang, S., Fletcher, W. H., and Johnson, D. A. (1995) Regulation of cAMP-dependent protein kinase: enzyme activation without dissociation, *Biochemistry 34*, 6267−6271.

BI0354435